

Simultaneous Functionalization of Methane and Carbon Dioxide Mediated by Single Platinum Atomic Anions

Gaoxiang Liu, Isuru R. Ariyaratna, Sandra M. Ciborowski, Zhaoguo Zhu, Evangelos Miliordos,* and Kit H. Bowen*



Cite This: *J. Am. Chem. Soc.* 2020, 142, 21556–21561



Read Online

ACCESS |



Metrics & More

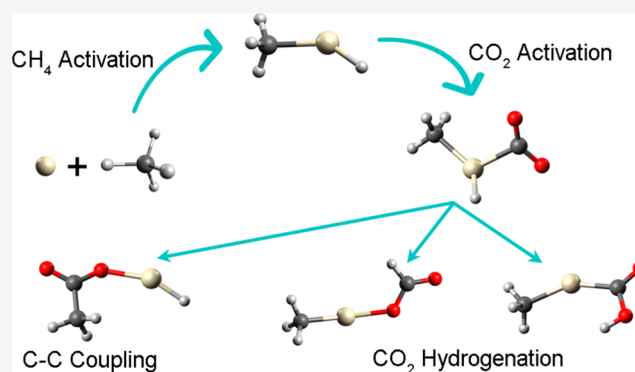


Article Recommendations



Supporting Information

ABSTRACT: Mass spectrometric analysis of the anionic products of interaction among Pt^- , methane, and carbon dioxide shows that the methane activation complex, $\text{H}_3\text{C-Pt-H}^-$, reacts with CO_2 to form $[\text{H}_3\text{C-Pt-H}(\text{CO}_2)]^-$. Two hydrogenation and one C–C bond coupling products are identified as isomers of $[\text{H}_3\text{C-Pt-H}(\text{CO}_2)]^-$ by a synergy between anion photoelectron spectroscopy and quantum chemical calculations. Mechanistic study reveals that both CH_4 and CO_2 are activated by the anionic Pt atom and that the successive depletion of the negative charge on Pt drives the CO_2 insertion into the Pt–H and Pt–C bonds of $\text{H}_3\text{C-Pt-H}^-$. This study represents the first example of the simultaneous functionalization of CH_4 and CO_2 mediated by single atomic anions.



INTRODUCTION

The transformation of the two abundant C_1 feedstocks, methane and carbon dioxide, into functional molecules is of great interest for environmental and economic reasons. A long-sought goal has been a mutual transformation in which methane and carbon dioxide directly functionalize each other so as to be simultaneously converted.¹ For example, $-\text{H}$ and $-\text{CH}_3$ groups, the active species from the breakage of one C–H bond of methane, may, respectively, couple with CO_2 to form higher value products. This process, however, is rather challenging due to the high stability of both methane and carbon dioxide.² The end product of methane and carbon dioxide conversion is usually the generation of syngas by methane dry reforming, but this indirect route consumes large amounts of energy.³ Several catalysts, including metal-exchanged zeolites,⁴ Cu/Co metal oxides,⁵ and oxide-supported noble metals,⁶ have been explored for the direct mutual functionalization of methane and carbon dioxide. Nevertheless, these catalytic processes require high temperature and suffer from poor yield and selectivity. The major challenge is rooted in the demand for catalysts to simultaneously tackle methane activation, which is oxidative, and carbon dioxide conversion, which is reductive. Recent gas-phase studies have shown that small clusters such as CuB^+ and RhVO_3^- mediate the direct conversion of methane with carbon dioxide.⁷ Atoms in these clusters take different roles in interacting with methane or carbon dioxide, while they work cooperatively as a whole reaction site to finish the reactions. Here, we aim to further reduce the size of the reaction site,

addressing the mutual functionalization of methane and carbon dioxide mediated by single atomic anions.

We had originally been inspired by a lineage of our recent studies. In one study, we show that platinum atomic anions, Pt^- , selectively activate one C–H bond in methane to form a $\text{H}_3\text{C-Pt-H}^-$ complex. The methyl and the hydro groups are expected to be reactive to other small molecules, establishing the basis for further methane functionalization.⁸ In other studies related to CO_2 activation and hydrogenation, we demonstrate that negatively charged metal atoms, including Pt^- , activate CO_2 ^{9,10} and that metal hydrides, especially platinum hydrides, hydrogenate CO_2 into formate.^{11,12} On the basis of these findings, we conceive that Pt^- is active in both the oxidative methane activation and the reductive CO_2 functionalization and that by coupling such reactivities, Pt^- can mediate the mutual transformation of methane and carbon dioxide. In this study, we show that Pt^- breaks a methane molecule into $-\text{H}$ and $-\text{CH}_3$ groups and couples the two groups, respectively, with CO_2 to form formate and acetate adducts. This work represents the first example of the mutual functionalization of methane and carbon dioxide mediated by single atoms.

Received: October 25, 2020

Published: December 14, 2020



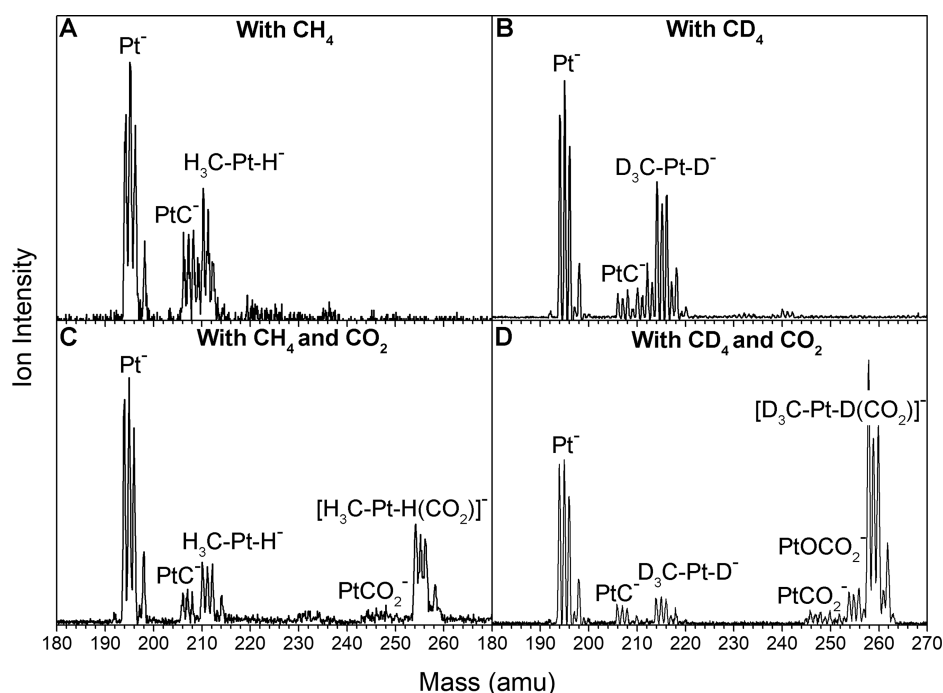


Figure 1. Mass spectra of Pt⁻ with methane (A), with deuterated methane (B), with methane and carbon dioxide (C), and with deuterated methane and carbon dioxide (D).

RESULTS AND DISCUSSION

The mutual functionalization of methane and CO₂ starts with the selective activation of one C–H bond in methane by single platinum anions. Methane activation occurred in a laser vaporization source, where the laser ablated Pt⁻ reacted with methane or deuterated methane introduced into the vaporization chamber. The activation products, PtCH₄⁻ and PtCD₄⁻, were, respectively, characterized by anion photoelectron spectroscopy and confirmed as H₃C–Pt–H⁻ and D₃C–Pt–D⁻ (Figure S1, ref 8). These activation products then reacted with CO₂ added into a reaction cell downstream. The resultant mass spectra show prominent mass series of [H₃C–Pt–H(CO₂)]⁻ and [D₃C–Pt–D(CO₂)]⁻ (Figure 1). Their isotopic patterns deviate from that of Pt due to mass overlaps with PtC⁻ or PtO⁻. The formation of PtC⁻ and PtO⁻ was likely due to trace amounts of carbon and oxygen present on the platinum metal surface or due to the carbon and oxygen existed in the laser vaporization housing which were released when interacting with the plasma. The strong ion intensities of [H₃C–Pt–H(CO₂)]⁻ and [D₃C–Pt–D(CO₂)]⁻ suggest an efficient interaction between CO₂ and the methane activation complexes.

We then applied anion photoelectron spectroscopy to characterize [H₃C–Pt–H(CO₂)]⁻ and [D₃C–Pt–D(CO₂)]⁻ (Figure 2). The photoelectron spectra were taken at all but the lowest-mass isotopes of the interested anions, because the lowest-mass peaks may overlap with peaks of PtC(CO₂)⁻ or PtO(CO₂)⁻. No significant spectroscopic difference was observed among the spectra taken for the same species. Here, we present a representative spectrum, respectively, for [H₃C–Pt–H(CO₂)]⁻ and [D₃C–Pt–D(CO₂)]⁻. The fact that Figure 2A,B have essentially identical features confirms that [H₃C–Pt–H(CO₂)]⁻ and [D₃C–Pt–D(CO₂)]⁻ have the same geometries and electronic structures. By examining the electron binding energies (EBE) of the spectral features, we obtain the vertical detachment energies, VDE, of these reaction

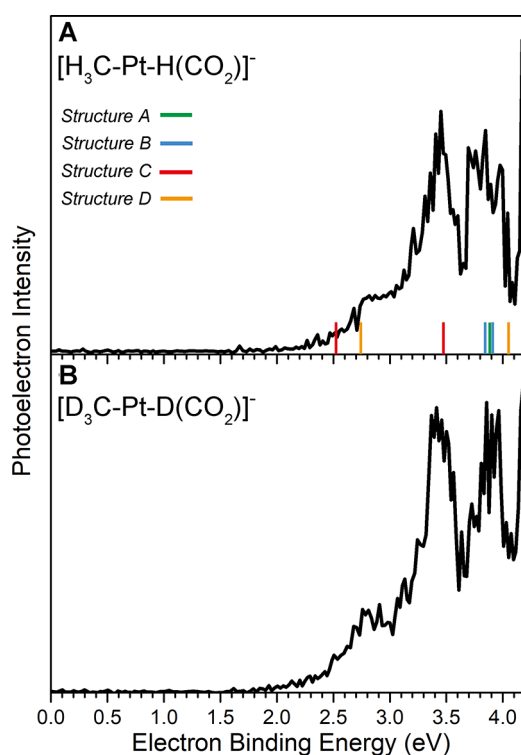


Figure 2. Photoelectron spectra of [H₃C–Pt–H(CO₂)]⁻ (A) and [D₃C–Pt–D(CO₂)]⁻ (B), both measured with 266 nm (4.661 eV) photons. The stick spectrum overlay represents the calculated VDEs of different [H₃C–Pt–H(CO₂)]⁻ structures in Figure 3.

products. The VDE is defined as the photodetachment transition energy at which the Franck–Condon overlap is at its maximum between the anion’s vibrational wave function and that of its neutral counterpart. The feature from 2.4 to 3.0 eV is broad with its peak less discernible, suggesting

contributions from multiple photodetachment transitions. The peaks at higher EBE yields VDE values of 3.41, 3.90, and 4.18 eV for $[\text{H}_3\text{C-Pt-H}(\text{CO}_2)]^-$ and $[\text{D}_3\text{C-Pt-D}(\text{CO}_2)]^-$.

Density functional theory (DFT) calculations were performed to find $[\text{H}_3\text{C-Pt-H}(\text{CO}_2)]^-$ isomers that are possibly prepared via the reaction between $\text{H}_3\text{C-Pt-H}^-$ and CO_2 . The energetics of these isomers were then refined at the CCSD(T) level of theory. The optimized geometries for these reaction products are presented in Figure 3 along with their

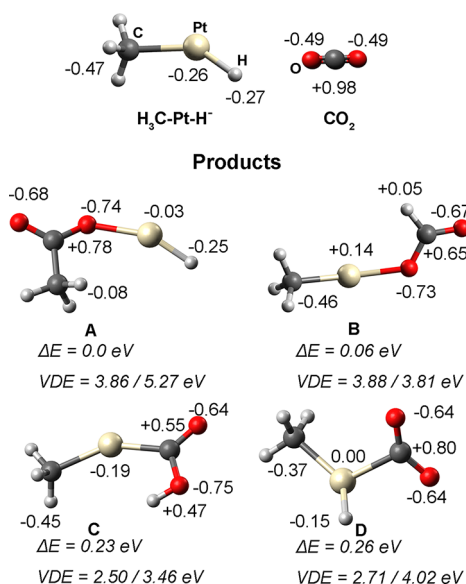


Figure 3. Optimized structures for $\text{H}_3\text{C-Pt-H}^-$, CO_2 , and $[\text{H}_3\text{C-Pt-H}(\text{CO}_2)]^-$. The relative energies of $[\text{H}_3\text{C-Pt-H}(\text{CO}_2)]^-$ and their calculated VDEs to singlet and triplet neutrals are shown below each structure. The Natural Bond Orbital (NBO) charge on each atom is also provided. The charge besides the methyl groups shows the total charge on $-\text{CH}_3$.

relative energies. All energies are zero-point corrected. The structures of $\text{H}_3\text{C-Pt-H}^-$ and CO_2 are also provided for reference. All $[\text{H}_3\text{C-Pt-H}(\text{CO}_2)]^-$ structures have a doublet electronic state. The global minimum of $[\text{H}_3\text{C-Pt-H}(\text{CO}_2)]^-$, **A**, features hydro and acetate groups, respectively, attached to the Pt atom, yielding a $\text{H}_3\text{CCOO-Pt-H}^-$ structure. In this structure, CO_2 is inserted into the Pt-C bond of $\text{H}_3\text{C-Pt-H}^-$ and couples its carbon atom with the methyl group to form an acetate. In structure **B**, which is only 0.06 eV higher in energy than the global minimum, CO_2 is wedged into the Pt-H bond of $\text{H}_3\text{C-Pt-H}^-$ to form a $\text{H}_3\text{C-Pt-OCOH}^-$, that is, CO_2 is hydrogenated to formate. In structure **C**, CO_2 is also hydrogenated, but the H atom is attached to the O atom, forming a $\text{H}_3\text{C-Pt-COOH}^-$ structure. Structure **D** is obtained by the CO_2 chemisorption onto the Pt atom in $\text{H}_3\text{C-Pt-H}^-$. In structure **D**, CO_2 is significantly bent, suggesting that CO_2 is activated on the Pt site.

A distinct advantage for gas-phase experiments is the combination of experimental characterization and state-of-the-art quantum chemistry calculations to identify reaction intermediates and products, laying the foundation for a mechanistic insight into the reactions at a molecular level.¹³ To verify these calculated structures, we calculated their VDEs at the CCSD(T) level of theory and compared them with the experimental values (Figures 2 and 3). The EBE transition from 2.5 to 2.9 eV results from the photodetachment

transitions of structures **C** and **D**, the calculated VDEs of which to their singlet neutrals are 2.50 and 2.71 eV, respectively. The EBE feature that peaked at 3.41 eV matches the calculated VDE of structure **C** to its triplet neutral counterpart, further confirming structure **C** as one of the reaction products. According to calculations on the excited state energies, this spectral feature also has contribution from the photodetachment transition of structure **C** to the first excited state of its singlet neutral counterpart (Table S1). Meanwhile, the EBE peak at 4.15 eV is attributed to the photodetachment transition of structure **D** to its triplet neutral. Therefore, structure **D** is also confirmed as a reaction product. Structures **C** and **D** have no transitions with photodetachment energies around 3.9 eV (Table S1), suggesting that the 3.90 eV feature is due to structures **A** and **B**. Because structures **A** and **B** both have calculated VDEs that match the spectroscopic feature at 3.87 eV, at this point, we only conclude that at least one of them exists in the reaction products.

We investigated the reaction pathway using quantum calculations to resolve the uncertainty in identifying all reaction products and to provide mechanistic insight into the synergetic methane and CO_2 functionalization (Figure 4). The

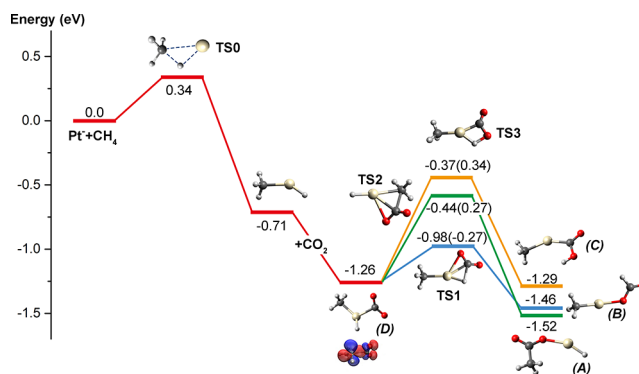


Figure 4. Profile of the tandem reaction between Pt^- , CH_4 , and CO_2 . Zero-point corrected energies are given in eV. The numbers in parentheses indicate the activation barriers compared to the entrance channel of CO_2 functionalization.¹⁴ The letters in parentheses correspond to their labels in Figure 3. The potential energy surface is referenced to the total energy of isolated Pt^- , CH_4 , and CO_2 .

reaction starts with the selective activation of one C-H bond in methane by Pt^- , which has been extensively studied in our previous work.⁸ This step includes a barrier of 0.34 eV and is exothermic by 0.71 eV. The resultant $\text{H}_3\text{C-Pt-H}^-$ interacts with CO_2 and binds it by forming a Pt-C bond (structure **D**). Concurrently, a total of 0.48 |e| negative charge is transferred to CO_2 . Such negative charge transfer is the first step of CO_2 functionalization. Therefore, both CH_4 and CO_2 are activated on the negatively charged Pt atom. After being activated, CO_2 can insert into the Pt-C or the Pt-H bond via three different routes for further functionalization. In the route with the lowest activation barrier, CO_2 interacts with the Pt-H bond of $\text{H}_3\text{C-Pt-H}^-$. The H atom transfers to the C atom while the Pt atom binds the O atom, leading to the formation of $\text{H}_3\text{C-Pt-OCOH}^-$ that contains a formate moiety (Structure **B**). The transition state, **TS1**, is located 0.27 eV below $\text{H}_3\text{C-Pt-H}^-$ and CO_2 , which is the entrance channel for the CO_2 functionalization step under our experimental conditions.¹⁴ Therefore, $\text{H}_3\text{C-Pt-H}^-$ readily hydrogenates CO_2 into the formate adduct, **B**, without apparent activation barriers. CO_2

can also insert into the Pt–C bond of $\text{H}_3\text{C–Pt–H}^-$ via TS2, where the C atom in CO_2 bonds with the C atom in the $-\text{CH}_3$ group. The activation barrier is 0.27 eV when compared to the energy of $\text{H}_3\text{C–Pt–H}^-$ and CO_2 . This route leads to $\text{H}_3\text{CCOO–Pt–H}^-$ (structure A), a C–C coupling product featuring an acetate group. In addition, the H atom of the Pt–H in $\text{H}_3\text{C–Pt–H}^-$ can transfer to the O atom, forming another CO_2 hydrogenation product (structure C). The activation barrier for this route is 0.34 eV. All these barriers are accessible under our experimental conditions where excess energy is provided via multicollisions with the fastest He molecules in the Maxwell–Boltzmann distribution.¹⁵ As mentioned earlier, the spectroscopic evidence alone can confirm the existence of structures C and D as reaction products but not structures A and B. The calculated reaction pathway helps resolve this uncertainty: both structures A and B are kinetically easier to form and thermodynamically more stable than structure C. Since structure C has been confirmed, structure A and B should also exist as reaction products. Therefore, the combined experimental and computational evidence confirms that both CO_2 hydrogenation and C–C bond coupling occur during the reaction.

When Pt^- activates CH_4 , it is electronically excited *in situ* to the $^4\text{G}(6s^25d^86p^1)$ state to fulfill the donor–acceptor model for σ -bond activation.^{8,13d} The negative charge on Pt reduces to $-0.26|e|$ after distributing to the $-\text{H}$ and the $-\text{CH}_3$ groups (Figure 3). The resultant $\text{H}_3\text{C–Pt–H}^-$ activates CO_2 by donating one of the 5d electron pairs on Pt to the antibonding orbital of CO_2 . When Pt activates CO_2 , the Pt/O interaction is kinetically less favorable than the Pt/C interaction due to the electrostatic repulsion between the negatively charged Pt and O atoms. When CO_2 activation is complete, all the negative charge on Pt drains to CO_2 and Pt becomes practically neutral (Figure 3, Structure D). This charge redistribution largely reduces the electrostatic repulsion between Pt and O and thus the kinetic barrier for CO_2 to be inserted into the Pt–H or the Pt–C bonds. As a result, CO_2 insertion occurs to form the more stable R–Pt–O–R' structures (Structures A and B), completing the simultaneous functionalization of CH_4 and CO_2 .

Besides the reaction path we showed in this work, we also investigated other paths for the tandem reactions among Pt^- , CH_4 , and CO_2 . Instead of activating CH_4 first, it is also possible to first interact Pt^- with CO_2 in the laser vaporization chamber and then react the prepared PtCO_2^- ^{8b} with CH_4 in the reaction cell. Computationally, this route is plausible (Figure S2). Experimentally, however, no spectroscopic evidence was found for CO_2 hydrogenation or C–C bond coupling products: only structure D and a $\text{PtCO}_2^-(\text{CH}_4)$ physisorbed complex were confirmed (Figure S3). This suggests that in the reaction cell, PtCO_2^- overcomes the first barrier to activate CH_4 but not the second one for CO_2 insertion. We think this is because the short reaction time provided by our reaction cell, which is usually on the order of microseconds, is not enough for reactants to overcome multiple activation barriers. This route, however, may be feasible under other reaction environments such as in an ion trap. Reaction paths that involve breaking the C=O bond in CO_2 or more than one C–H bonds in CH_4 are impossible under our experimental conditions due to high kinetic barriers or low thermodynamic stability of the reaction products (Figures S2 and S4).

CONCLUSIONS

To summarize, we demonstrate for the first time that the single atomic Pt^- can mediate the mutual functionalization between CH_4 and CO_2 . The combined mass spectrometry, photoelectron spectroscopy, and quantum chemical calculation study reveals that the CH_4 activation complex, $\text{H}_3\text{C–Pt–H}^-$, interacts with CO_2 to form two hydrogenation and one C–C bond coupling products. Specifically, Pt^- breaks CH_4 into $-\text{H}$ and $-\text{CH}_3$, activates CO_2 , and couples the activated CO_2 , respectively, with $-\text{H}$ and $-\text{CH}_3$ to form formate and acetate products. Mechanistic analysis confirms the charge redistribution as the driving force for the CO_2 insertion step. The demonstration of the simultaneous CH_4 and CO_2 functionalization by atomic anions sheds light on new routes in the design of novel catalysts to utilize these two abundant C1 feedstocks.

METHODS

Experimental Methods. Anion photoelectron spectroscopy is conducted by crossing a beam of mass-selected negative ions with a fixed-frequency photon beam and energy-analyzing the resultant photodetached electrons. The photodetachment process is governed by the energy-conserving relationship: $h\nu = \text{EBE} + \text{EKE}$, where $h\nu$ is the photon energy, EBE is the electron binding energy, and EKE is the electron kinetic energy. Our apparatus consists of a laser vaporization cluster anion source with an attached ligation cell, a time-of-flight mass spectrometer, a Nd:YAG photodetachment laser (operating at 266 nm), and a magnetic bottle electron energy analyzer with a resolution is ~ 35 meV at 1 eV EKE.¹⁶ Photoelectron spectra were calibrated against the well-known atomic transitions of atomic Cu^- . The tandem reaction among Pt^- , methane (CH_4 , CD_4), and CO_2 was studied using a laser vaporization/reaction cell arrangement.¹⁷ Atomic platinum anions were generated by laser vaporization of a pure platinum foil wrapped around an aluminum rod. The resultant plasma was cooled with 5% CH_4 or CD_4 helium gas mixture delivered by a pulsed valve, having a backing pressure of 60 psig. The resulting $\text{H}_3\text{C–Pt–H}^-$ or $\text{D}_3\text{C–Pt–D}^-$ then traveled through a reaction cell (4 mm diameter, 5 cm length), where it encountered CO_2 . CO_2 was introduced into the reaction cell by a second pulsed valve, backed by 15 psig of pure CO_2 gas. The resulting $[\text{H}_3\text{C–Pt–H}(\text{CO})_2]^-$ and $[\text{D}_3\text{C–Pt–D}(\text{CO})_2]^-$ anionic clusters were then mass-analyzed and mass-selected by the time-of-flight mass spectrometer and their photoelectron spectra measured.

Computational Methods. All Density functional theory (DFT) calculations were performed with Gaussian16 package.¹⁸ Geometry optimizations were carried out with the B3LYP functional and the aug-cc-pVTZ (H, C, O)^{19,20} || aug-cc-pVTZ-PP (Pt)²¹ basis sets. Stuttgart relativistic pseudopotential was employed to replace 60 inner electrons ($1s^22s^22p^63s^23p^63d^{10}4s^24p^64d^{10}4f^{14}$) of the Pt atom.²¹ All geometry optimization calculations were followed by frequency calculations to verify that intermediate structures are real minima in the potential energy surface by confirming that their frequencies are real. Transition states that connect these intermediates bear only one imaginary frequency.

More accurate results were obtained by performing single point CCSD(T)²² calculations using the DFT/B3LYP optimized structures. The same basis set was applied. Zero-point energies collected from DFT/B3LYP calculations were added to the CCSD(T) energies. MOLPRO 2015²³ was used to perform all CCSD(T) calculations.

ASSOCIATED CONTENT

Supporting Information

The Supporting Information is available free of charge at <https://pubs.acs.org/doi/10.1021/jacs.0c11112>.

Coordinates and vibrational frequencies of all structures (PDF)

AUTHOR INFORMATION

Corresponding Authors

Kit H. Bowen – Department of Chemistry, Johns Hopkins University, Baltimore, Maryland 21218, United States; orcid.org/0000-0002-2858-6352; Email: kbowen@jhu.edu

Evangelos Miliordos – Department of Chemistry and Biochemistry, Auburn University, Auburn, Alabama 36849, United States; orcid.org/0000-0003-3471-7133; Email: ezm0048@auburn.edu

Authors

Gaoxiang Liu – Department of Chemistry, Johns Hopkins University, Baltimore, Maryland 21218, United States; orcid.org/0000-0002-1001-0064

Isuru R. Ariyaratna – Department of Chemistry and Biochemistry, Auburn University, Auburn, Alabama 36849, United States

Sandra M. Ciborowski – Department of Chemistry, Johns Hopkins University, Baltimore, Maryland 21218, United States; orcid.org/0000-0001-9453-4764

Zhaoguo Zhu – Department of Chemistry, Johns Hopkins University, Baltimore, Maryland 21218, United States

Complete contact information is available at:

<https://pubs.acs.org/10.1021/jacs.0c11112>

Notes

The authors declare no competing financial interest.

ACKNOWLEDGMENTS

The experimental part of this material was supported by the Air Force Office of Scientific Research (AFOSR) under grant number, FA9550-19-1-0077 (KHB). IRA and EM are indebted to Auburn University (AU) for financial support. This work was completed with resources provided by the Auburn University Hopper Cluster and Alabama Supercomputer Center.

REFERENCES

- (1) Havran, V.; Dudukovic, M. P.; Lo, C. S. Conversion of methane and carbon dioxide to higher value products. *Ind. Eng. Chem. Res.* **2011**, *50* (12), 7089–7100.
- (2) Gunsalus, N. J.; Koppaka, A.; Park, S. H.; Bischof, S. M.; Hashiguchi, B. G.; Periana, R. A. Homogeneous functionalization of methane. *Chem. Rev.* **2017**, *117* (13), 8521–8573.
- (3) (a) Shi, L.; Yang, G.; Tao, K.; Yoneyama, Y.; Tan, Y.; Tsubaki, N. An introduction of CO₂ conversion by dry reforming with methane and new route of low-temperature methanol synthesis. *Acc. Chem. Res.* **2013**, *46* (8), 1838–1847. (b) Pakhare, D.; Spivey, J. A review of dry (CO₂) reforming of methane over noble metal catalysts. *Chem. Soc. Rev.* **2014**, *43* (22), 7813–7837.
- (4) (a) Wang, X.; Qi, G.; Xu, J.; Li, B.; Wang, C.; Deng, F. NMR-spectroscopic evidence of intermediate-dependent pathways for acetic acid formation from methane and carbon monoxide over a ZnZSM-5 zeolite catalyst. *Angew. Chem., Int. Ed.* **2012**, *51* (16), 3850–3853. (b) Wu, J.-F.; Yu, S.-M.; Wang, W. D.; Fan, Y.-X.; Bai, S.; Zhang, C.-W.; Gao, Q.; Huang, J.; Wang, W. Mechanistic insight into the formation of acetic acid from the direct conversion of methane and carbon dioxide on zinc-modified H-ZSM-5 zeolite. *J. Am. Chem. Soc.* **2013**, *135* (36), 13567–13573. (c) Rabie, A. M.; Betiha, M. A.; Park, S.-E. Direct synthesis of acetic acid by simultaneous co-activation of methane and CO₂ over Cu-exchanged ZSM-5 catalysts. *Appl. Catal., B* **2017**, *215*, 50–59.
- (5) Huang, W.; Xie, K.-C.; Wang, J.-P.; Gao, Z.-H.; Yin, L.-H.; Zhu, Q.-M. Possibility of direct conversion of CH₄ and CO₂ to high-value products. *J. Catal.* **2001**, *201* (1), 100–104.
- (6) (a) Wilcox, E. M.; Roberts, G. W.; Spivey, J. J. Direct catalytic formation of acetic acid from CO₂ and methane. *Catal. Today* **2003**, *88* (1–2), 83–90. (b) Ding, Y.-H.; Huang, W.; Wang, Y.-G. Direct synthesis of acetic acid from CH₄ and CO₂ by a step-wise route over Pd/SiO₂ and Rh/SiO₂ catalysts. *Fuel Process. Technol.* **2007**, *88* (4), 319–324.
- (7) (a) Chen, Q.; Zhao, Y. X.; Jiang, L. X.; Chen, J. J.; He, S. G. Coupling of methane and carbon dioxide mediated by diatomic copper boride cations. *Angew. Chem., Int. Ed.* **2018**, *57* (43), 14134–14138. (b) Yang, Y.; Yang, B.; Zhao, Y. X.; Jiang, L. X.; Li, Z. Y.; Ren, Y.; Xu, H. G.; Zheng, W. J.; He, S. G. Direct Conversion of Methane with Carbon Dioxide Mediated by RhVO₃[−] Cluster Anions. *Angew. Chem.* **2019**, *131* (48), 17447–17452. (c) Zhao, Y.-X.; Yang, B.; Li, H.-F.; Zhang, Y.; Yang, Y.; Liu, Q.-Y.; Xu, H.-G.; Zheng, W.-J.; He, S.-G. Photoassisted Selective Steam and Dry Reforming of Methane to Syngas Catalyzed by Rhodium-Vanadium Bimetallic Oxide Cluster Anions at Room Temperature. *Angew. Chem., Int. Ed.* **2020**, *59*, 21216–21223.
- (8) Liu, G.; Zhu, Z.; Ciborowski, S. M.; Ariyaratna, I. R.; Miliordos, E.; Bowen, K. H. Selective Activation of the C-H Bond in Methane by Single Platinum Atomic Anions. *Angew. Chem.* **2019**, *131* (23), 7855–7859.
- (9) Zhang, X.; Lim, E.; Kim, S. K.; Bowen, K. H. Photoelectron spectroscopic and computational study of (M-CO₂)[−] anions, M= Cu, Ag, Au. *J. Chem. Phys.* **2015**, *143* (17), 174305.
- (10) Liu, G.; Ciborowski, S. M.; Zhu, Z.; Chen, Y.; Zhang, X.; Bowen, K. H. The metallo-formate anions, M(CO₂)[−], M= Ni, Pd, Pt, formed by electron-induced CO₂ activation. *Phys. Chem. Chem. Phys.* **2019**, *21* (21), 10955–10960.
- (11) Zhang, X.; Liu, G.; Meiwes-Broer, K. H.; Ganteför, G.; Bowen, K. CO₂ activation and hydrogenation by PtH_n[−] cluster anions. *Angew. Chem.* **2016**, *128* (33), 9796–9799.
- (12) Liu, G.; Poths, P.; Zhang, X.; Zhu, Z.; Marshall, M.; Blankenhorn, M.; Alexandrova, A. N.; Bowen, K. H. CO₂ Hydrogenation to Formate and Formic Acid by Bimetallic Palladium-Copper Hydride Clusters. *J. Am. Chem. Soc.* **2020**, *142* (17), 7930–7936.
- (13) (a) Zhou, S.; Li, J.; Schlangen, M.; Schwarz, H. Bond activation by metal-carbene complexes in the gas phase. *Acc. Chem. Res.* **2016**, *49* (3), 494–502. (b) Schwarz, H.; Shaik, S.; Li, J. Electronic effects on room-temperature, gas-phase C-H Bond activations by cluster oxides and metal carbides: The methane challenge. *J. Am. Chem. Soc.* **2017**, *139* (48), 17201–17212. (c) Zhao, Y.-X.; Li, Z.-Y.; Yang, Y.; He, S.-G. Methane activation by gas phase atomic clusters. *Acc. Chem. Res.* **2018**, *51* (11), 2603–2610. (d) Armentrout, P. Activation of CH₄ by Gas-Phase Mo⁺, and the Thermochemistry of Mo- ligand Complexes. *J. Phys. Chem. A* **2006**, *110* (27), 8327–8338. (e) Green, A. E.; Justen, J.; Schöllkopf, W.; Gentleman, A. S.; Fielicke, A.; Mackenzie, S. R. IR Signature of Size-Selective CO₂ Activation on Small Platinum Cluster Anions, Pt_n[−] (n= 4–7). *Angew. Chem.* **2018**, *130* (45), 15038–15042. (f) Johnson, G. E.; Mitric, R.; Nössler, M.; Tyo, E. C.; Bonacic-Koutecky, V.; Castleman, A., Jr. Influence of charge state on catalytic oxidation reactions at metal oxide clusters containing radical oxygen centers. *J. Am. Chem. Soc.* **2009**, *131* (15), 5460–5470. (g) Deng, G.; Pan, S.; Wang, G.; Zhao, L.; Zhou, M.; Frenking, G. Beryllium Atom Mediated Dinitrogen Activation via Coupling with Carbon Monoxide. *Angew. Chem., Int. Ed.* **2020**, *59*, 18201–18207. (h) Jian, J.; Wu, X.; Chen, M.; Zhou, M. Boron-Mediated Carbon-Carbon Bond Cleavage and Rearrangement of Benzene Forming the Borepinyl Radical and Borole Derivatives. *J. Am. Chem. Soc.* **2020**, *142*, 10079–10086.
- (14) Under our experiment conditions, where CH₄ activation and CO₂ functionalization occurred in separated cells, H₃C-Pt-H[−] was sufficiently cooled when they exited the laser vaporization cell and entered the reaction cell, that is, the energy released during the exothermic CH₄ activation had dissipated before H₃C-Pt-H[−] interacting with CO₂. Therefore, when calculating the activation

barriers for the CO₂ functionalization step, the total energy of H₃C-Pt-H⁻ and isolated CO₂ should be referenced. For other reactors such as ion traps, it is more reasonable to reference to the total energy of Pt⁻, CH₄, and CO₂ for all steps in the reaction.

(15) (a) Liu, G.; Ciborowski, S. M.; Zhu, Z.; Bowen, K. H. Activation of hydroxylamine by single gold atomic anions. *Int. J. Mass Spectrom.* **2019**, *435*, 114–117. (b) Lang, S. M.; Bernhardt, T. M.; Chernyy, V.; Bakker, J. M.; Barnett, R. N.; Landman, U. Selective C-H bond cleavage in methane by small gold clusters. *Angew. Chem.* **2017**, *129* (43), 13591–13595.

(16) Zhang, X.; Liu, G.; Ganteför, G.; Bowen, K. H.; Alexandrova, A. N. PtZnH₅⁻, A σ -aromatic cluster. *J. Phys. Chem. Lett.* **2014**, *5* (9), 1596–1601.

(17) (a) Liu, G.; Ciborowski, S. M.; Bowen, K. H. Photoelectron spectroscopic and computational study of pyridine-ligated gold cluster anions. *J. Phys. Chem. A* **2017**, *121* (31), 5817–5822. (b) Liu, G.; Miliordos, E.; Ciborowski, S. M.; Tschurl, M.; Boesl, U.; Heiz, U.; Zhang, X.; Xantheas, S. S.; Bowen, K. Communication: Water activation and splitting by single metal-atom anions. *J. Chem. Phys.* **2018**, *149* (22), 221101.

(18) Frisch, M. J.; Trucks, G. W.; Schlegel, H. B.; Scuseria, G. E.; Robb, M. A.; Cheeseman, J. R.; Scalmani, G.; Barone, V.; Petersson, G. A.; Nakatsuji, H.; Li, X.; Caricato, M.; Marenich, A. V.; Bloino, J.; Janesko, B. G.; Gomperts, R.; Mennucci, B.; Hratchian, H. P.; Ortiz, J. V.; Izmaylov, A. F.; Sonnenberg, J. L.; Williams-Young, D.; Ding, F.; Lipparini, F.; Egidi, F.; Goings, J.; Peng, B.; Petrone, A.; Henderson, T.; Ranasinghe, D.; Zakrzewski, V. G.; Gao, J.; Rega, N.; Zheng, G.; Liang, W.; Hada, M.; Ehara, M.; Toyota, K.; Fukuda, R.; Hasegawa, J.; Ishida, M.; Nakajima, T.; Honda, Y.; Kitao, O.; Nakai, H.; Vreven, T.; Throssell, K.; Montgomery, J. A., Jr.; Peralta, J. E.; Ogliaro, F.; Bearpark, M. J.; Heyd, J. J.; Brothers, E. N.; Kudin, K. N.; Staroverov, V. N.; Keith, T. A.; Kobayashi, R.; Normand, J.; Raghavachari, K.; Rendell, A. P.; Burant, J. C.; Iyengar, S. S.; Tomasi, J.; Cossi, M.; Millam, J. M.; Klene, M.; Adamo, C.; Cammi, R.; Ochterski, J. W.; Martin, R. L.; Morokuma, K.; Farkas, O.; Foresman, J. B.; Fox, D. J. Gaussian, Inc., Wallingford CT, 2016.

(19) Kendall, R. A.; Dunning, T. H.; Harrison, R. J. Electron Affinities of the First-row Atoms Revisited. Systematic Basis Sets and Wave Functions. *J. Chem. Phys.* **1992**, *96* (9), 6796–6806.

(20) Dunning, T. H. Gaussian Basis Sets for Use in Correlated Molecular Calculations. I. The Atoms Boron through Neon and Hydrogen. *J. Chem. Phys.* **1989**, *90* (2), 1007–1023.

(21) Figgen, D.; Peterson, K. A.; Dolg, M.; Stoll, H. Energy-Consistent Pseudopotentials and Correlation Consistent Basis Sets for the 5d Elements Hf-Pt. *J. Chem. Phys.* **2009**, *130* (16), 164108.

(22) Raghavachari, K.; Trucks, G. W.; Pople, J. A.; Head-Gordon, M. A Fifth-Order Perturbation Comparison of Electron Correlation Theories. *Chem. Phys. Lett.* **1989**, *157* (6), 479–483.

(23) Werner, H.-J.; Knowles, P. J.; Knizia, G.; Manby, F. R.; Schütz, M.; Celani, P.; Györffy, W.; Kats, D.; Korona, T.; Lindh, R.; Mitrushekov, A.; Rauhut, G.; Shamasundar, K. R.; Adler, T. B.; Amos, R. D.; Bernhardsson, A.; Berning, A.; Cooper, D. L.; Deegan, M. J. O.; Dobbyn, A. J.; Eckert, F.; Goll, E.; Hampel, C.; Hesselmann, A.; Hetzer, G.; Hrenar, T.; Jansen, G.; Köppl, C.; Liu, Y.; Lloyd, A. W.; Mata, R. A.; May, A. J.; McNicholas, S. J.; Meyer, W.; Mura, M. E.; Nicklass, A.; O'Neill, D. P.; Palmieri, P.; Peng, D.; Pflüger, K.; Pitzer, R.; Reiher, M.; Shiozaki, T.; Stoll, H.; Stone, A. J.; Tarroni, R.; Thorsteinsson, T.; Wang, M., see <https://www.molpro.net>.